Journal of Experimental Botany, Vol. 59, No. 11, pp. 3051–3068, 2008
doi:10.1093/jxb/ern154 Advance Access publication 4 July, 2008
This paper is available online free of all access charges (see http://jxb.oxfordjournals.org/open_access.html for further details)

Journal of Experimental Botany
www.jxb.oxfordjournals.org

RESEARCH PAPER

Clathrin-dependent and independent endocytic pathways in tobacco protoplasts revealed by labelling with charged nanogold

Elisabetta Onelli[1], Cristina Prescianotto-Baschong[2], Marco Caccianiga[1] and Alessandra Moscatelli[1,*]

[1] *Department of Biology, University of Milan, Milan, Italy*

[2] *Department of Biochemistry, Biozentrum, University of Basel, Basel, Switzerland*

Received 28 February 2008; Revised 3 April 2008; Accepted 8 May 2008

Abstract

Positively charged nanogold was used as a probe to trace the internalization of plasma membrane (PM) domains carrying negatively charged residues at an ultrastructural level. The probe revealed distinct endocytic pathways within tobacco protoplasts and allowed the morphology of the organelles involved in endocytosis to be characterized in great detail. Putative early endosomes with a tubulo-vesicular structure, similar to that observed in animal cells, are described and a new compartment, characterized by interconnected vesicles, was identified as a late endosome using the *Arabidopsis* anti-syntaxin family Syp-21 antibody. Endocytosis dissection using Brefeldin A (BFA), pulse chase, temperature- and energy-dependent experiments combined with quantitative analysis of nanogold particles in different compartments, suggested that recycling to the PM predominated with respect to degradation. Further experiments using ikarugamycin (IKA), an inhibitor of clathrin-dependent endocytosis, and negatively charged nanogold confirmed that distinct endocytic pathways coexist in tobacco protoplasts.

Key words: Charged nanogold, endocytosis, membrane recycling, *Nicotiana tabacum*, protoplasts, vesicle trafficking.

Introduction

Endocytosis is involved in many cellular processes, such as nutrient uptake, the down-regulation of plasma membrane (PM) receptors, and PM recycling and signalling. The endocytic pathway is known to intersect secretory and biosynthetic processes during recycling to the PM and protein transport to lysosomes or vacuoles (Henkel *et al*., 1996; Ang *et al*., 2004). Endocytosis has been extensively studied in animals and the organelles involved defined by ultrastructure and specific protein–lipid domain composition. Mechanisms of endocytosis involving clathrin-dependent or independent internalization have been characterized and shown to coexist in animal cells (Baba *et al*., 2001; Nichols and Lippincot-Schwartz, 2001; Kirkham *et al*., 2005) as well as in plants, where receptor-mediated internalization (Holstein, 2002), phagocytosis (Son *et al*., 2003) and fluid phase endocytosis (Baluška *et al*., 2004) have been observed. Identification of plant structural sterols and lipid rafts suggests that endocytic processes, similar to fluid phase or caveolae/lipid raft-mediated endocytosis in animals (Borner *et al*., 2005; Martin *et al*., 2005), may also be active in plants. Understanding of the mechanisms regulating endocytosis in plants lags far behind that of animals. Studies of plant endocytosis using cationized ferritin as a probe have revealed the ultrastructure of some membraneous compartments involved in internalization and trafficking during receptor-mediated endocytosis (Tanchak *et al*., 1984; Samuels and Bisalputra, 1990; Fowke *et al*., 1991). Some of these organelles were found to be ultrastructurally similar in animal and plant cells. In animals, vesicles derived from the PM during receptor-mediated endocytosis were delivered to a first compartment which was considered to be a sorting station for internalized molecules. This compartment was defined as early endosome or sorting endosome in animal cells and as partially

* To whom correspondence should be addressed. E-mail: alessandra.moscatelli@unimi.it

Abbreviations: BFA, Brefeldin A; ER, endoplasmic reticulum; IKA, Ikarugamycin; MVBs, multivesicular bodies; PCR, partially coated reticulum; PM, plasma membrane; PVCs, prevacuolar compartments; TGN, trans Golgi network.

coated reticulum (PCR) in plants (Pesacreta and Lucas, 1985; Tanchak *et al*., 1988). In animals, early endosomes were regarded as a mosaic of membrane domains whose specific protein–lipid composition enabled them to sort molecules for degradation from those for recycling to the PM in the vesicular and tubular portions of the early endosome, respectively (Gruenberg, 2001). Recycling of proteins and lipids to the PM seems to involve two distinct populations of endosomes with specific biochemical composition: early and tubular recycling endosomes (Sheff *et al*., 1999). Tubular recycling endosomes are involved in the slower pathway of recycling to the PM (Sheff *et al*., 1999), while in the fast pathways, proteins and lipids can return directly to the cell surface from the early compartments without the involvement of recycling endosomes (Hao and Maxfield, 2000).

In plants, there is still no clear evidence of early endosomes ultrastructure or of recycling endosomes, although an intense recycling pathway to the PM has been detected using styryl FM dyes as probes (Ueda *et al*., 2001). However, in animals and plants, the degradation pathway seems to involve production of multivescicular bodies (MVBs) by early endosomes. In animals, MVBs are thought to originate from the vesicular portion of early endosomes and to fuse or mature into late endosomes and finally to fuse with lysosomes. In plants, the degradative pathway seems to involve the maturation of early into late endosomes (Ueda *et al*., 2001) which have been identified as MVBs or prevacuolar compartments (PVCs). MVBs/PVCs are known to be involved in both the secretory and endocytic pathways (Tse *et al*., 2004): plant PVCs are considered an intermediate for delivering proteins to storage vacuoles and for sorting materials to lytic compartments (Jiang and Rogers, 1998). Direct fusion of PVCs with vacuoles without involvement of vesicle transfer has been hypothesized, as suggested for lysosomes in animals (Luzio *et al*., 2000; Gruenberg and Stenmark, 2004). However, proteins and lipids can also recycle back from late endosomes to the PM or other endocytic organelles through the trans-Golgi network (TGN) (Goda and Pfeffer, 1988; Uemura *et al*., 2004). In animals receptor-mediated endocytosis may intersect fluid phase or clathrin-independent endocytosis in early endosomes or TGN (Gruenberg, 2001), whereas in plants there is no information about how different endocytic pathways interact with each other and with secretory or biosynthetic pathways. Besides the TGN (Kim *et al*., 2001), endosomes also seem to have functional interactions with the Golgi apparatus and the endoplasmic reticulum (ER; Jiang and Rogers, 1998).

Fluorescent probes (Baluška *et al*., 2002; Bolte *et al*., 2004) have recently been used to study vesicle trafficking in living plant cells. Although FM-dyes are extremely useful to trace the internalization of PM and endosome transport (Bolte *et al*., 2004), showing endocytosis in the cell, they do not allow the process to be dissected or discrimination of different endocytic pathways. Most probes used for ultrastructural studies only trace receptor-mediated endocytosis.

In order to investigate the complexity of endocytic pathways in tobacco protoplasts, positively charged nanogold has been used as a marker (Prescianotto-Baschong and Riezman, 1998). Positively charged nanogold is relatively small (about 1 nm) and is not degraded in acidic compartments (unlike cationized ferritin and biotinylated-BSA). This probe binds to negatively charged residues on the cell surface irrespective of their molecular nature. Combined with freeze substitution protocols, they allowed multiple endocytic pathways to be determined and the ultrastructural morphology of endocytic organelles of plant cells to be characterized in great detail.

Time-course experiments and use of *Arabidopsis thaliana* anti-syntaxin SYP21 antiserum (daSilva Conceição *et al*., 1997; Sanderfoot *et al*., 1998) as the specific marker in immunolabelling experiments allowed an internalization pathway that partially overlaps with receptor-mediated endocytosis to be defined. Pulse chase, temperature- and energy-dependent experiments, use of BFA, and quantitative analysis of nanogold particles in different compartments showed that recycling to the PM predominated over degradation. Use of IKA, an inhibitor of clathrin-dependent endocytosis (Hasumi *et al*., 1992; Luo *et al*., 2001), and negatively charged nanogold that binds different PM components with respect to positively charged nanogold, confirmed that distinct endocytic pathways are active in tobacco protoplasts.

Materials and methods

Tobacco cell culture and preparation of protoplasts

Tobacco cells were grown in a culture chamber at 25±2 °C with continuous lighting for 7 d. MS medium containing 0.1 mg ml^{-1} myo-inositol, 0.5 mg ml^{-1} thiamine chlorohydrate, 0.5 mg ml^{-1} glycine, 0.5 mg ml^{-1} nicotinic acid, 0.5 mg ml^{-1} pyridoxine, 8.84 mg ml^{-1} 2,4-dichlorophenoxyacetic acid, and 20 g l^{-1} sucrose was used.

Protoplasts (8 g) were obtained by digesting cell walls with 20 ml digestion solution (0.45 M pH, 5.5 mannitol, 1.5% cellulase, 0.15% pectinase and protease inhibitors) for 3 h at room temperature. Protoplasts were then filtered (100 μm mesh), centrifuged at 380 *g* for 3 min and resuspended in 10 ml culture medium with 0.45 M mannitol and protease inhibitors for 15 min before nanogold addition.

Time-course experiments and electron microscope analysis

For time-course experiments, protoplasts were incubated with 30 nmol of positively charged nanogold (Nanoprobes, New York, USA) and resuspended into 200 μl distilled water (MilliQ grade). Samples were taken at 5, 15, 30, 45, and 120 min. Protoplasts were fixed overnight at 4 °C by direct addition of formaldehyde and glutaraldehyde to final concentrations of 2% and 0.2%, respectively, or with glutaraldehyde 2%. In all experiments, cell viability was checked by staining protoplasts with FDA (Heslop-Harrison and Heslop-Harrison, 1970) before fixation. Samples were then observed by fluorescence microscopy (Leica DMRD). After fixation,

specimens were centrifuged at 380/400 *g* for 3 min and resuspended with an equal volume of 2% low melting agarose in HEPES buffer (50 mM HEPES, 1 mM $MgCl_2$, 5 mM EGTA) to form solidified drops, which were rinsed for 1 h in HEPES buffer. Protoplasts were treated with ammonium chloride 50 mM in HEPES for 30 min at room temperature and dehydrated with increasing concentrations of methanol. Infiltration and polymerization were done at low temperature (–20 °C) with a CS-Auto (Reichert Jung, London England) cryo-substitution apparatus, according to the protocols furnished with LR GOLD resin (London Resin, London England).

80 nm ultra-thin sections, obtained using an Ultracut E microtome (Reichert Jung), were collected on nickel grids. Positively and negatively charged nanogold was enhanced with QH silver (Nanoprobes) as described by the manufacturer for 2 min in time-course and control experiments and for 1 min for immunogold labelling. Sections were then stained with 3% uranyl-acetate for 20 min and observed with a Jeol SX100 (Jeol, Tokyo, Japan) electron microscope at 80 kV.

Quantitation of positively and negatively charged nanogold in different compartments was performed counting the number of gold particles observed at a fixed magnification of 20 000 of the electron microscope. Total numbers obtained for different labelled protoplast profiles were used to calculate the percentage of nangold internalized in different membraneous compartments. Standard errors (SE) were calculated for all the experiments using positively or negatively charged nanogold for graphs. ANOVA test was used to evaluate the difference between single compartments in different experimental conditions and between different incubation times in the time-course and pulse experiments. Tukey's Post Hoc test of Honestly Significant Difference (HSD) was used to assess the significance of each comparison.

Pulse chase

In pulse chase experiments protoplasts were incubated for 15 min (T_0) with 30 nmol of nanogold and then particles were removed from the medium. Samples were centrifuged at 380/400 *g* for 3 min, resuspended in 10 ml culture medium with 0.45 M mannitol and protease inhibitors without the probe. They were fixed and embedded after 15 min and 45 min.

Azide treatment and temperature controls

For energy controls, protoplasts were pretreated for 2 min with different concentrations of sodium azide (1, 5, 100, 500 μM) before addition of positively charged nanogold.

For low temperature experiments, protoplasts were incubated at 4 °C for 30 min before addition of positively charged nanogold. Samples were taken after incubation with the probe for 45 min at 4 °C. Recovery of intracellular traffic after low temperature incubation was performed by bringing protoplasts to room temperature and taking samples after 15 min and 45 min.

Dissection of the endocytic process by BFA and IKA

Protoplasts were preincubated for 30 min with 1 or 10 μM BFA and with 5 μM IKA. Positively charged nanogold was then added. Samples were processed after 45 min. Since BFA and IKA were suspended in DMSO, to evaluate the possible effect of DMSO control experiments were done in which protoplasts were preincubated with 1 and 2 μl ml^{-1} DMSO.

Protoplast crude extract

For protoplast crude extracts, cells were homogenized in 2 vols of PEM buffer (100 mM PIPES pH 6.8, 5 mM EGTA, 1 mM $MgCl_2$, 1 mM DTT, 1 mM PMSF, 10 μg ml^{-1} TAME, 10 μg ml^{-1} leupeptin, 10 μg ml^{-1} pepstatin A, 4 μM aprotinin, and 8 μM antipain) using a 2 ml Potter homogenizer on ice. Laemmli sample buffer (LSB) was added to the homogenate and the sample was boiled for 5 min. It was subsequently centrifuged at 4 °C for 36 min at 15 000 rpm in an A21C ALC rotor. The resulting supernatant was collected as crude extract.

SDS-PAGE and western blot

Proteins were denatured with LSB and separated on 8% polyacrylamide gels following the method of Laemmli (1970). Electrophoresis reagents were obtained from Bio-Rad Laboratories (CA, USA). Gels were stained with Coomassie blue. Western blot was performed according to Towbin *et al*. (1979). Syp-21 antiserum (kindly supplied by Dr NV Raikhel, University of California, Riverside, USA; daSilva Conceicxao et al., 1997; Sanderfoot et al., 1998) was used at a final dilution of 1:2000. As secondary antibody, peroxidase conjugated goat anti-rabbit (1:10 000, final dilution) was purchased from Amersham Biosciences. Detection of the antibodies was performed as outlined in the Amersham ECL kit booklet. All gels and western blot images were scanned with an Epson Expression 1680 PRO and combined using Adobe Photoshop.

Immunoelectron microscopy

For immunogold experiments, after silver enhancement of positively charged nanogold (1 min), sections were saturated with 2% BSA in TBS and then incubated with SYP21 primary antibody (1:200). After rinses in 0.1% BSA/TBS, sections were incubated with anti-rabbit secondary antibody conjugated with 20 nm gold particles (BBI International, Cardiff, UK). Specimens were stained with 3% uranyl-acetate for 20 min. Observations were made with a Jeol SX100 (Jeol, Tokyo, Japan) electron microscope at 80 kV.

Results

Time-course experiments with positively charged nanogold

The positively charged nanogold was used in time-course experiments in order to observe the endocytic pathway and destination of internalized PM in tobacco protoplasts. The cryo-substitution embedding procedure allowed the ultrastructure of membraneous compartments involved in endocytosis to be defined. The fixation procedure contained a higher concentration of formaldehyde than glutaraldehyde to facilitate tracing of the immunolabelling procedure. The granulose appearance of the cytoplasm does not seem to be a consequence of fixation since a control experiment using only glutaraldehyde did not give different results (data not shown).

In time-course experiments, nanogold particles were incubated with protoplasts in culture medium and samples were taken at different times; the presence of the probe in vesicles and membraneous compartments was revealed as dark spots by silver enhancement (Figs 1, 2). Quantitative analysis showed an increase in the total number of gold particles in cells mostly during the first 30 min since between 5 min and 15 min and between 30 min and 120 min no significant variation was observed (ANOVA test; Fig. 3A).

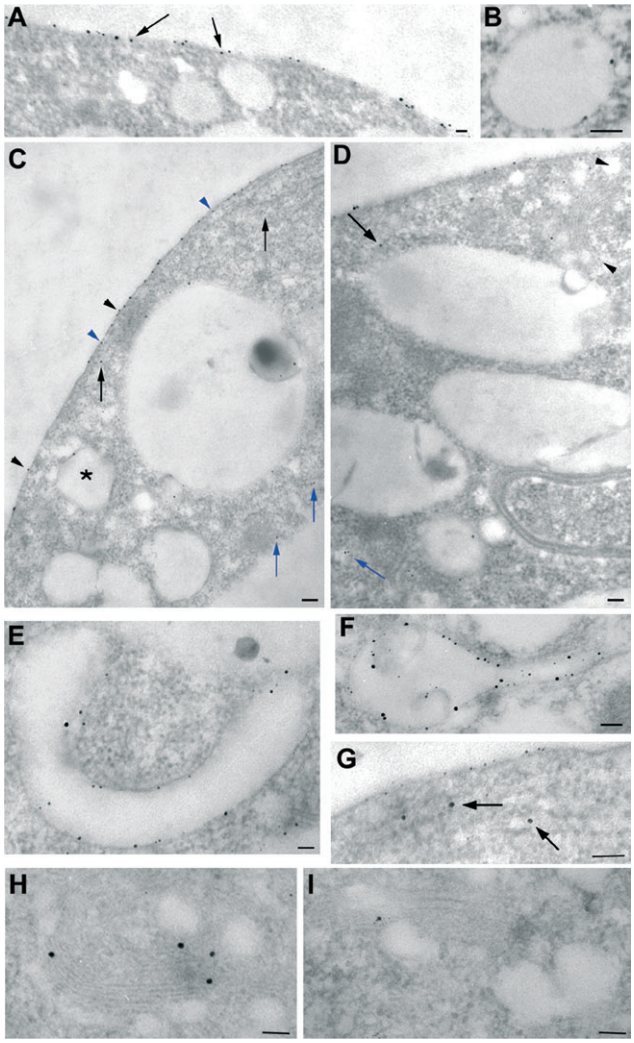

Fig. 1. Compartments labelled by positively charged nanogold during time-course experiments: protoplasts were incubated with 30 nmol of positively charged nanogold and fixed after 5, 15, 30, 45, and 120 min. (A) After 5 min of incubation most of the particles were distributed on the PM and peripheral vesicles (arrows). (B) Some large vesicles near the PM appeared labelled by the probe. (C, D) After 5–120 min of incubation, the probe was seen in small vesicles immediately below the PM (C, see blue arrowheads for peripheral vesicles and black arrowheads for PM) and into inner vesicles in the cortical region of cell (C, D, see black arrows) or deeper in the cytoplasm (C, D, see blue arrows). Golgi bodies appeared labelled by the probe (D, see arrowheads). (E) After 15–120 min of incubation, positively charged nanogold was seen inside large tubular membraneous compartments (large vesicles). (F) Some roundish-tubular vesicles showed internal membranes similar to MVBs labelled by the probe. (G, H, I) The ER (G, arrow) and Golgi bodies (H, I) also contained gold particles. (A, B, E, F, G, H, I) Bar=50 nm. (C, D) Bar=100 nm.

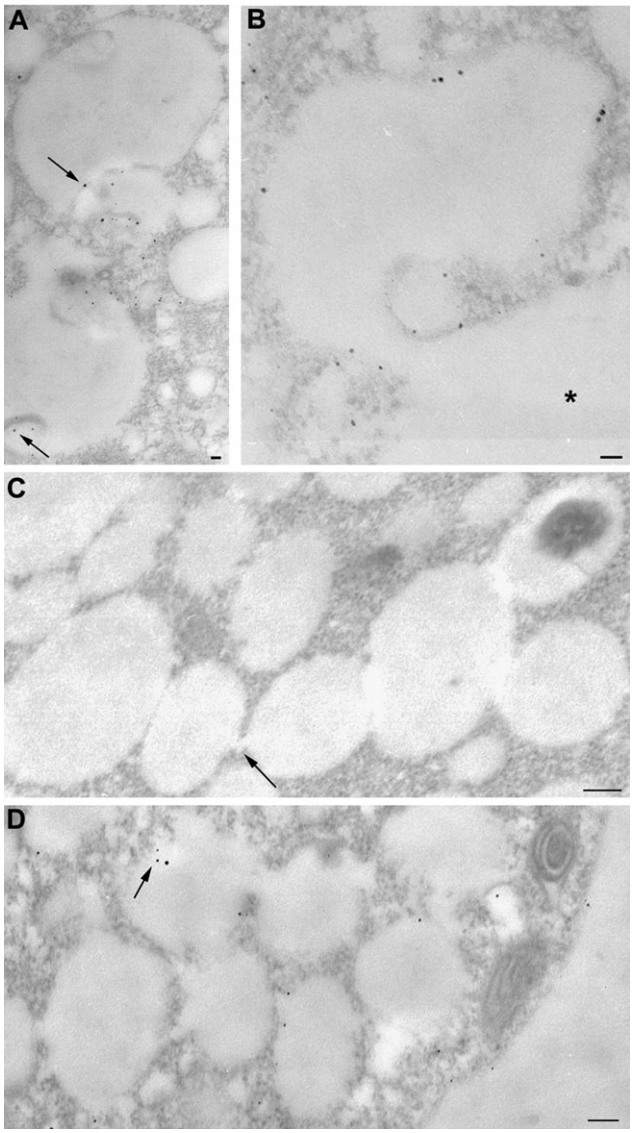

Fig. 2. Compartments labelled by positively charged nanogold during time-course experiments. (A, B) Labelled MVB fusing with the vacuole (*). The particles were seen in MVBs (see arrows). (C) No nanogold staining was observed in systems of interconnected vesicles forming a single compartment after 15 min of incubation in time-course experiments (arrow: interconnections). (D) Labelling appeared in these compartments after 30 min of incubation with positively charged nanogold and gold particles appeared to detach from the membrane (see arrows). Bar=100 nm.

Time-course experiments showed that binding of nanogold to the PM was immediate. After 5 min most of the nanogold was localized on the PM (Fig. 1A). In the cytoplasm, the probe was seen in small vesicles (about 20 nm), immediately below the PM (henceforth 'peripheral vesicles'; Fig. 1A, C) and in vesicles having diameters ranging from 50–100 nm in the cortical region of cell ('inner vesicles'; Fig. 1C, D; black arrows). Only occasionally was a small amount of nanogold observed in large vesicles (200–700 nm) near the PM (Fig. 1B, C); here gold particles were bound to the inner face of membrane vesicles (Fig. 1B). Quantitative analysis showed many particles in peripheral vesicles after 5 min incubation (Fig. 3B). Less probe was detected in inner compartments, as large and inner vesicles localized in the cortical area of the cytoplasm, at least at this time (Fig. 3B). Very few particles were associated with the tonoplast.

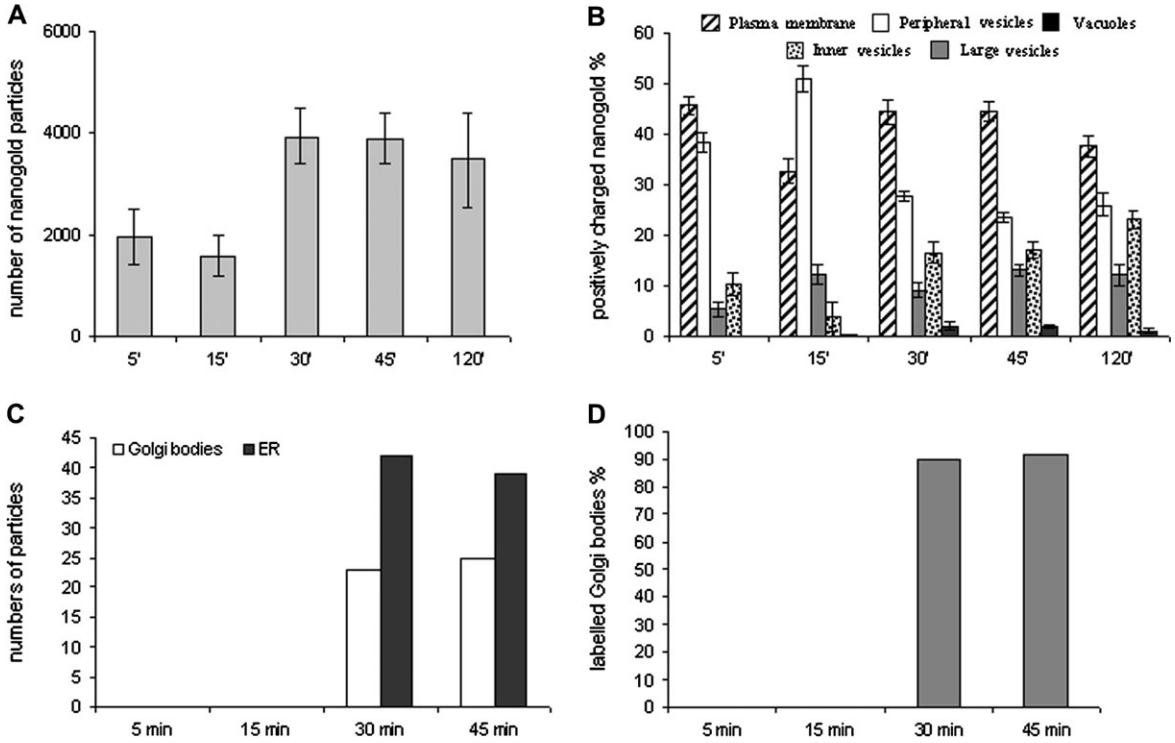

Fig. 3. Quantitative analysis during time-course experiments. (A) Variation in total amount of nanogold particles counted in samples during the time-course. (B) Positively charged nanogold was quantified in different compartments by counting the number of gold particles observed at a fixed magnification of 20 000 in the electron microscope. Total numbers obtained for 10 labelled protoplast profiles were used to calculate the percentage of nangold internalized in different membraneous compartments. Standard error (SE) is shown at each point of the time-course experiments. (C) Gold particles counted in the Golgi and ER. These compartments were labelled after 30 min of incubation. (D) Percentage of labelled Golgi bodies.

The pattern of internalization was different at 15 min of incubation (Fig. 3B). At this time, positively charged nanogold was still found on the PM, but most of particles were at the periphery of the cells (Tukey's HSD test $P < 0.01$), probably due to fast entry of nanogold bound to the PM or to fast nanogold recycling by small vesicles. Labelled small vesicles were observed in peripheral/cortical regions of protoplasts and in small vesicles deeper in the cytoplasm (50–100 nm, also considered 'inner vesicles'; Fig. 1C, D, blue arrows), probably playing a role in membrane trafficking from the cell periphery to other compartments. The decrease in gold content in inner vesicles ($P < 0.01$; Fig. 3B) suggests that cortical vesicles could be involved before large vesicles in the transport of internalized material since, at this time, the contribution of deeper small vesicles to the quantity of probe was still modest. By internal trafficking, nanogold particles entered large tubular (diameter about 200 nm; Fig. 1E) and round membraneous compartments (200–700 nm; 'large vesicles'; Fig. 1B,C). Quantitative analysis during the time-course experiment showed an increase in probe in this compartment between 5 min and 45 min; (Tukey's HSD test $P=0.013$; Fig. 3B) suggesting that the latter could be an early membraneous target for endocytic vesicles originating at the PM. This tubular/round compartment could be a site of particle collection before sorting. Some MVBs (with size ranging from 200 nm to 500 nm as already observed; Tse *et al*., 2004; Foresti *et al*., 2006; Haas *et al*., 2007), were labelled and gold particles were associated with both the delimiting and internal membranes (Fig. 2A). These multivesicular structures often extended into a tubular portion (Fig. 1F) suggesting that the compartments described as tubular vesicles and MVBs could actually be parts of or derived from the same organelle.

In specific areas of the cell, systems of interconnected vesicles ranging from 200 nm to 800 nm, sometimes containing electron dense material, were observed to form a single compartment (Fig. 2C, D). No nanogold staining was observed in this compartment after 15 min of incubation (Fig. 2C), whereas after 30 min of incubation nanogold particles were observed (Fig. 2D), suggesting that this membrane network was involved later in endocytosis.

After 30 min the number of particles decreased in peripheral vesicles ($P < 0.01$), while increased significantly on the PM ($P < 0.05$) and in all the inner compartments (Fig. 3B). At 45 min and 120 min (Fig. 3B) the pattern of distribution and morphology of compartments were similar to that observed after 30 min suggesting that an equilibrium in gold particle distribution was reached.

During the time-course experiment, the number of nanogold particles remained low in the central vacuole, compared to other compartments, although an increase was observed after 30 min of incubation (P <0.01; Fig. 3B). Nanogold was associated with the inner face of the tonoplast and smaller vacuole-like compartments (larger than 1 μm). Free gold particles were only occasionally observed inside vacuoles (data not shown). Sometimes MVBs with internal vesicles labelled by the probe appeared to fuse with the tonoplast of the vacuole (Fig. 2A, B). Membraneous organelles, such as the endoplasmic reticulum (ER; Fig. 1G) and Golgi bodies (Fig. 1D, H, I), appeared to be labelled by the probe after 30 min of incubation and more than 90% of Golgi bodies were labelled (Fig. 3C, D). Labelled small vesicles were present throughout the cytoplasm suggesting their involvement in internal trafficking (Fig. 1C, D).

To avoid artefacts due to silver enhancement, protoplasts which were not incubated with nanogold were processed as reported above: no labelling was observed in the cytoplasm or membraneous organelles (Fig. 4A). Since tobacco protoplasts are extremely fragile, after each treatment they were tested for viability with FDA which was also a useful method to test membrane integrity (Fig. 4B, C). In time-course experiments and controls, about 95% of protoplasts showed FDA-dependent fluorescence suggesting that cell membranes were intact and protoplasts viable. During TEM observations, dead or dying protoplasts were identified by the presence of many autophagic vacuoles. Many nanogold particles appeared widespread in the cytoplasm and cell organelles preventing quantitation analysis and the identification of endocytic compartments (data not shown). The percentage of the damaged cells with respect to intact cells was about 10%.

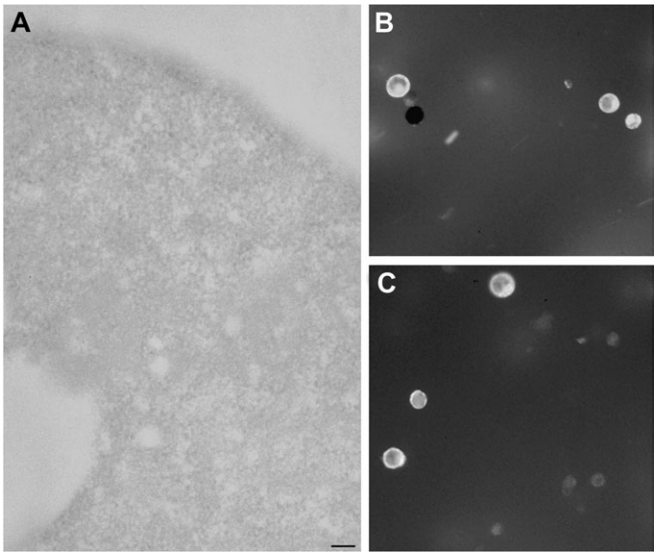

Fig. 4. (A) Controls of probe specificity: protoplasts incubated without nanogold were processed for silver enhancement and no dark spots were visible in the cells. (B, C) FDA test of protoplast viability after 120 min of incubation during the time-course experiments (B; M=55X) and after 500 μM sodium azide treatment (C; M=68X). In all samples, protoplasts showed FDA-dependent fluorescence, indicating intact cell membranes and viable protoplasts. Bar=50 nm.

Characterization of late compartments

After 30 min of incubation with nanogold, most membraneous organelles in the inner part of the cytoplasm were labelled by the probe. For this reason, to better define the nature of compartments that appeared to be involved late in nanogold internalization, a specific polyclonal antibody was used against a member of the syntaxin family isolated in *Arabidopsis* cells (Syp 21/AtPEP12p) (daSilva Conceição *et al*., 1997; Sanderfoot *et al*., 1998). This antibody is a marker of late endocytotic organelles (Tse *et al*., 2006).

The specificity of antibody was tested by western blot on crude extracts of tobacco protoplasts (Fig. 5A). The antibody recognized a single polypeptide of approximately 30 kDa, a molecular weight similar to the protein identified in *Arabidopsis* cells (36 kDa, daSilva Conceição *et al*., 1997) (Fig. 5, lane SYP21), while controls without primary antibody (Fig. 5, lane C) did not show any reaction. This antibody is therefore suitable for immunogold labelling experiments. To recognize nanogold from gold-conjugated antibodies, silver enhancement was performed for 1 min instead of 2 min. Nanogold particles were smaller than in the other experiments and smaller than the 20 nm gold particles bound to the antibody. Here Syp-21 antibody stained interconnected vesicle compartments (Fig. 5B; arrows indicate antibodies and arrowheads nanogold). Syp21 was also observed in nanogold-labelled MVBs (Fig. 5D; arrows indicate antibodies and arrowheads nanogold), often associated with the inner membrane. As observed in *Arabidopsis* (daSilva Conceição *et al*., 1997; Sanderfoot *et al*., 1998), organelles such as Golgi, ER, and tubular/round compartments were not labelled in tobacco protoplasts (data not shown). Controls without primary antibody did not show any labelling (Fig. 5C).

Pulse chase

During the time-course experiments, nanogold was continuously internalized at the PM. To define internal sorting and PM recycling of the probe better, pulse chase experiments were performed. At T_0 (15 min), as previously observed, most of the probe was localized at the cell periphery (Fig. 3B). After removing the probe, samples were taken after 15 min and 45 min. At 15 min, nanogold was more abundant in large (not significant) and inner vesicles (P <0.01) than at T_0 (Fig. 6A). Interestingly, 45 min after the pulse, the number of particles on the PM and in peripheral vesicles increased but decreased in inner

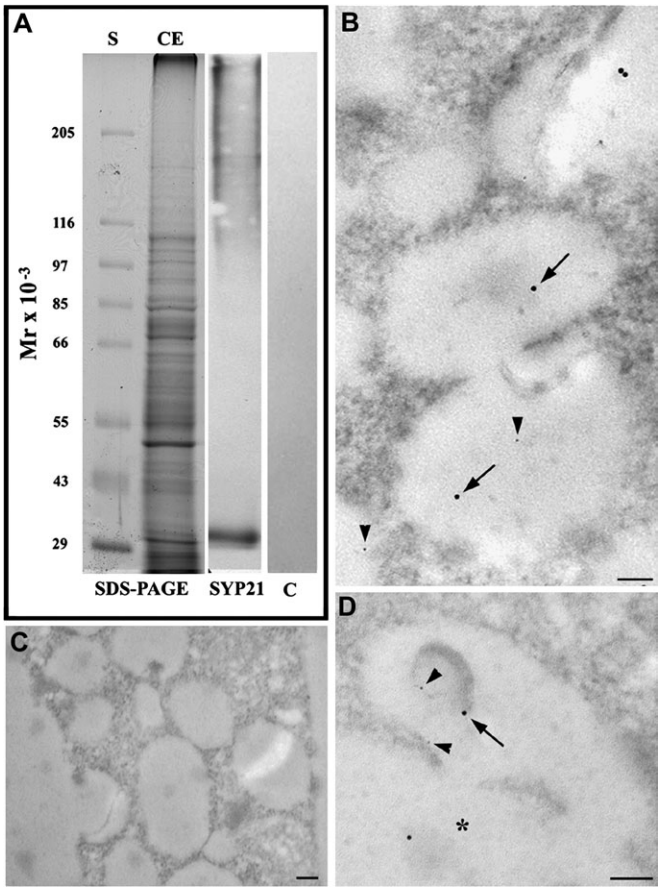

Fig. 5. Immunoblot and immunogold labelling by SYP21 polyclonal antibody, a marker of late endosomes. (A) The specificity of antibody was tested by western blot on tobacco protoplast crude extracts: lane CE showed SDS-PAGE of tobacco protoplast crude extract in which blot analysis using Syp 21 antibody (lane SYP21) specifically identified a single band at 30 kDa. Controls without primary antibody (lane C) did not show aspecific reactions. (B–D) In immunogold experiments, to distinguish the nanogold from gold-conjugated antibodies, the silver enhancement was performed for 1 min instead than 2 min. Nanogold particles were smaller than in the other experiments and smaller than the 20 nm gold particles bound to the secondary antibody. The antibody localized in interconnected vesicles (B; arrows) and MVBs (D, arrows) that were also labelled by nanogold (B, D, arrowheads). Multivesiculated vesicles fused with the central vacuole (asterisk). (C) Negative controls of immunogold analyses without primary antibody. No aspecific labelling was present. Bar=100 nm.

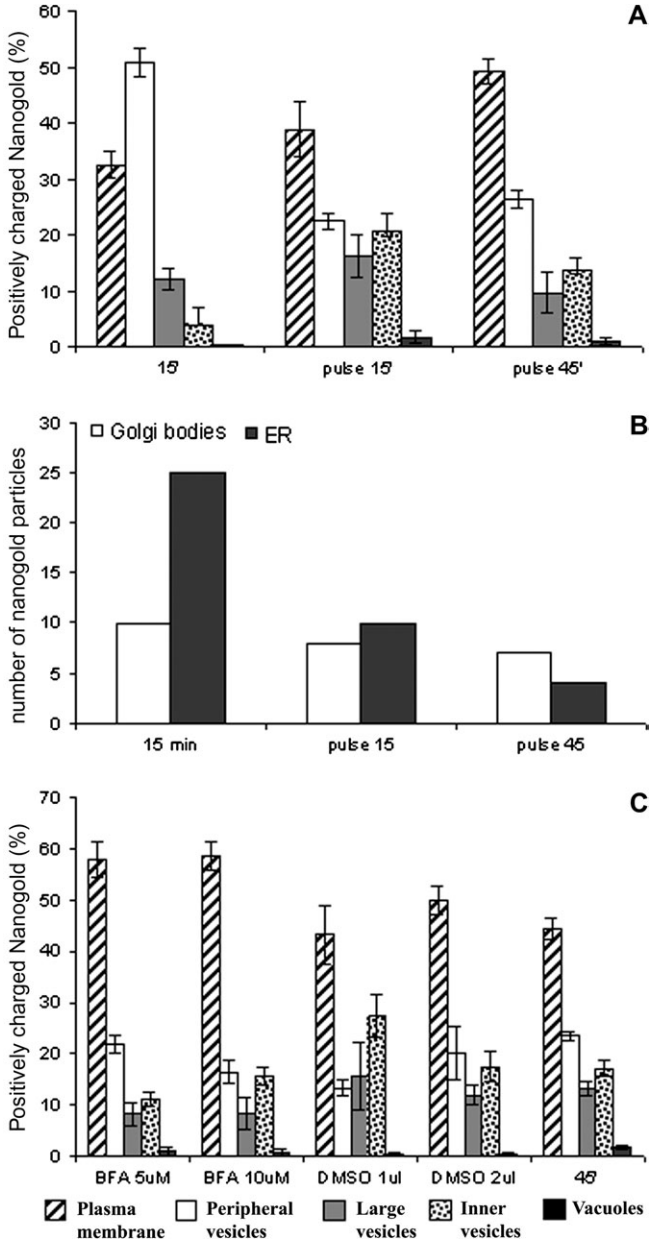

Fig. 6. Quantitative analysis in pulse, and BFA experiments. In pulse chase experiments (A, B) protoplasts were incubated for 15 min (T_0) with 30 nmol of nanogold and then particles were removed from the medium. Samples were fixed after 15 min and 45 min. (A) The percentage of nangold internalized in different membraneous compartments were calculated as described for the time-course experiments. Pulse experiments allowed the distribution of internalized nanogold within the cell compartments to be followed until 45 min, suggesting that recycling could be a prominent pathway with respect to degradation during nanogold endocytosis. In Golgi bodies and ER much less probe was observed (B) and the percentage of labelled Golgi bodies decreases with respect to the time-course. (C) Quantitative analysis showed that in BFA-treated tobacco protoplasts incubated with positively charged nanogold, BFA affected the early phases of the internalization process. Since BFA was dissolved in DMSO, BFA effects on nanogold internalization were compared with DMSO. Standard error (SE) is shown for each experiments.

cell compartments (P <0.01; Fig. 6A). Fifteen minutes after probe removal, the amount of gold in the central vacuoles increased, but after 45 min nanogold decreased on the tonoplast even if not significantly, suggesting that the probe was again entrained in vesicle traffic (Fig. 6A). Golgi bodies and ER were labelled by the probe but the amount of particles in this organelles was much lower with respect to the time-course (Fig. 6B).

Relation between exocytosis and endocytosis

The relation between exocytosis and membrane internalization was tested using BFA (Fig. 6C) which affects

membrane trafficking in mammalian cells (Nebenfuhr *et al.*, 2002) and disrupts Golgi organization in plants (Emans *et al.*, 2002). Control using DMSO seemed to affect the internalization process: in the presence of 1 μl ml^{-1} DMSO (Fig. 6C: corresponding to 5 μM BFA), a decrease in particles on the PM and in peripheral vesicles (P <0.01) was accompanied by an increase in large (P <0.05) and inner vesicles which could mean that DMSO enhanced traffic from peripheral vesicles to inner compartments and inhibited recycling to the PM (Fig. 6C: DMSO 1 μl ml^{-1}). The corresponding sample incubated with 5 μM BFA showed inhibition of uptake (P <0.05 on PM between 5 μM BFA and 1 μl ml^{-1} DMSO) and traffic from the periphery to the inner vesicles. In fact, the nanogold amount decreased in inner vesicles (P <0.05) and increased in peripheral vesicles (P <0.05), but not in large vesicles (not significant) with respect to the DMSO control (Fig. 6C: 5 μM BFA and DMSO 1 μl ml^{-1}). Increasing BFA concentration to 10 μM, did not induce a significant variations among compartments with respect to the control (Fig. 6C: 10 μM BFA and DMSO 2 μl ml^{-1}) suggesting that DMSO did not allow the BFA effects to be observed.

Azide treatment and low temperature affect endocytosis

To test for azide and temperature dependence of the endocytotic process, protoplasts were incubated with increasing concentrations of sodium azide (1, 5, 100, and 500 μM; Fig. 7A, B) to affect ATP production (Prescianotto-Baschong and Riezman, 1998) or kept at 4 °C for 30 min before probe addition (Fig. 7C, D). Although no changes in the morphology of compartments involved in gold transport were observed (data not show), quantitative analysis suggested that both sodium azide and temperature affected the endocytic process. At low sodium azide concentrations (1 μM and 5 μM; Fig. 7A) uptake of nanogold was not inhibited, but differences in the distribution of the probe were observed with respect to control (Fig. 7A). At 1 μM sodium azide, no significant changes in the distribution of nanogold were detected compared with the control (Fig. 7A; 45 min) whereas at 5 μM, the amount of probe increased in the inner vesicles (P <0.01) and decreased significantly in peripheral vesicles (P <0.05). High concentrations of sodium azide elicited different behaviours from low concentrations (Fig. 7B). An increase in particles on the PM and a decrease in large vesicles suggested that entry of the probe was inhibited (Fig. 7B) leading to a very low labelling in large vesicles (P <0.05).

The effect of temperature on uptake of nanogold was tested by adding probe to cells previously incubated at 4 °C for 30 min and kept at low temperature for a further 45 min (Fig. 7C). An increase in the number of particles was observed on the PM with respect to the control (not significant; Fig. 7C) and a corresponding increase in probe in peripheral vesicles (P <0.01) and a decrease in large vesicles was observed (P <0.01). During the recovery the incubation temperature was raised to 25 °C and samples were fixed after 15 min and 45 min at room temperature (Fig. 7D). The endocytic process seemed already to be reactivated after 15 min, since significant differences in probe distribution were not observed with respect to control experiments.

During sodium azide and cold treatments a very low level of labelling was observed in Golgi bodies and the ER compared to the control (45 min; Fig. 7E). At higher sodium azide concentrations, ER was never labelled, while Golgi bodies showed a decreased number of gold particles with respect to the lower sodium azide concentration. During the recovery from low temperature, an increased amount of particles was observed in Golgi bodies, suggesting a re-entry of the probe in vesicle trafficking (Fig. 7E). The percentage of labelled Golgi bodies decreased at high sodium azide (5 μM) with respect to that observed at low concentration (1 μM) and increased during the recovery from low temperature (Fig. 7F).

Positively charged nanogold internalization was affected by ikarugamycin

To confirm the presence of different nanogold endocytic pathways, the inhibitor of clathrin-dependent endocytosis, ikarugamycin (IKA) was used. Incubation with IKA affected the internalization of nanogold particles (Fig. 8). TEM observation showed that nanogold was mostly present on the PM (Fig. 8A), often in clusters, suggesting accumulation of probe at the peripheries of cells (Fig. 8A, see arrows). The abundance of nanogold on the cell surface and in the layer just under the PM made it difficult to distinguish labelling of the PM and of peripheral vesicles. However, incubation with IKA did not completely inhibit probe uptake, indicating that positively charged nanogold was internalized by more than one endocytic pathway. In fact, particles were also observed in interconnected large vesicles (Fig. 8B see arrows,) and MVBs (Fig. 8C, see arrows). Round/tubular structures were rarely labelled and no particles were observed in Golgi bodies or ER (data not shown). Quantitative analysis confirmed TEM observations (Fig. 8D). As for BFA, the effects of IKA treatment were compared with those observed when samples were treated with 1 μl ml^{-1} DMSO. IKA treatment induced greater accumulation of nanogold on the PM surface than in the control (DMSO 1 μl ml^{-1}; P <0.01) while large vesicles showed very few nanogold particles (P <0.05). A slight decrease in inner vesicles suggested that clathrin-independent processes are involved in this compartment.

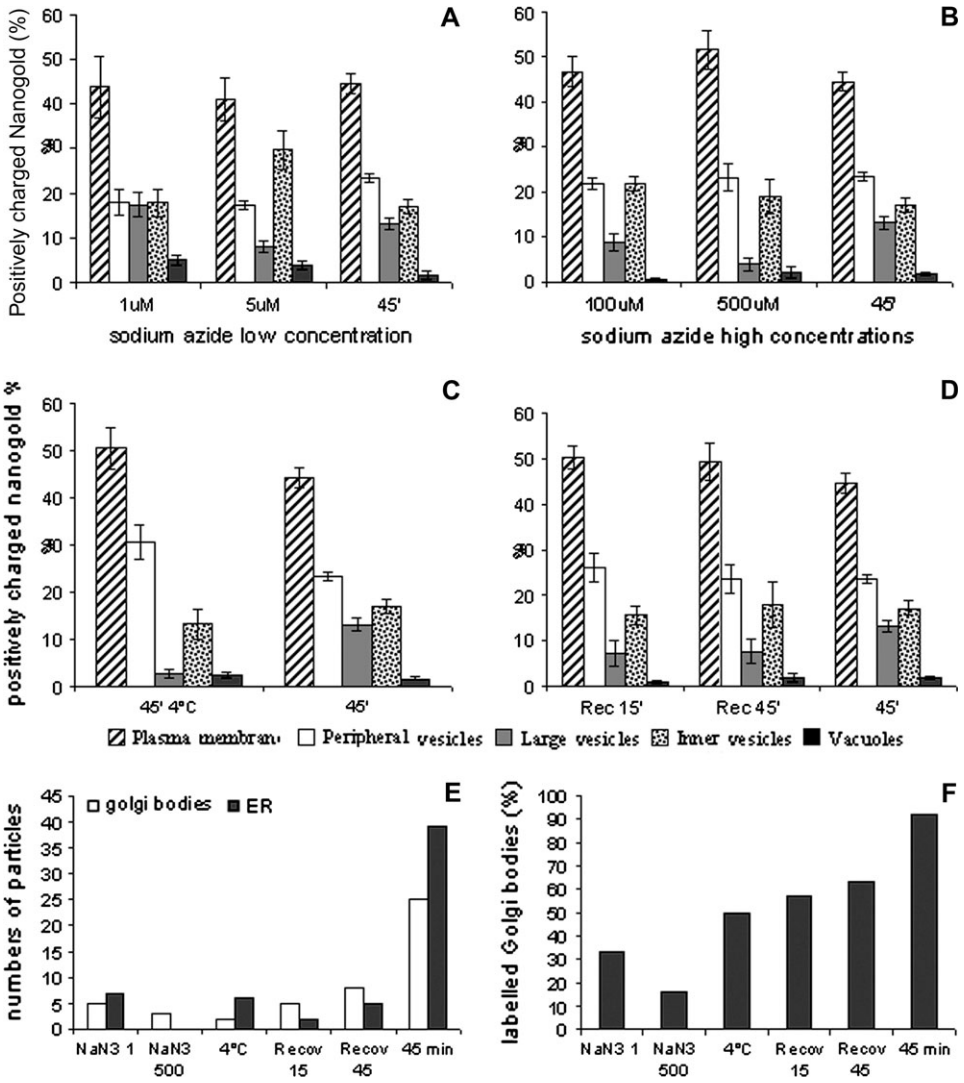

Fig. 7. Quantitation of the labelled profile during energy-dependent experiments and temperature-dependent experiments. (A, B) For energy controls, protoplasts were pretreated and incubated with different concentrations of sodium azide. (A) At low sodium azide concentrations uptake of nanogold was not inhibited but differences in the distribution of the probe were observed with respect to the control. (B) At high concentrations of sodium azide entry of probe was inhibited. (C) For low temperature experiments, protoplasts were incubated at 4 °C for 30 min before addition of positively charged nanogold and samples were taken after incubation with the probe for 45 min at 4 °C. An increase in the number of particles was observed on the PM with respect to the control and a corresponding decrease of probe was observed in peripheral and large vesicles. (D) Recovery of intracellular trafficking after incubation at low temperature was performed by bringing to 25 °C and taking samples after 15 min and 45 min. Quantitation data suggested that, during recovery, internalization was not reactivated while the recycling pathways was restored. The increase of the probe in inner vesicles and in vacuoles was due to the recovery of vesicle trafficking. (E, F) Effect of sodium azide and low temperature on Golgi and ER labelling. Sodium azide and cold experiments showed that a very low level of labelling was observed in Golgi bodies and ER (E) and a low percentage of Golgi bodies were labelled (F) compared to the control. Standard error (SE) is shown for each experiments.

Negatively charged nanogold confirmed the presence of different internalization pathways and of recycling to PM

Time-course experiments with negatively charged nanogold confirmed the presence of several endocytotic processes (Fig. 9). Since differently charged nanogold interacted with different PM molecules, it was presumed they could follow different internalization pathways, although partial overlapping could not be excluded.

Fewer negatively charged particles bound to the PM and localized in cells than positively charged nanogold, (P <0.01; Fig. 9A). A slight increase in internalized negatively charged nanogold was observed after 15 min, remaining almost constant after 30 min and 45 min, suggesting equilibrium between uptake and recycling of PM segments bound to the probe or, alternatively, saturation of PM sites binding negatively charged particles. Less probe was observed after 120 min incubation, suggesting that nanogold could have an inhibitory effect on endocytosis by this time. This time was therefore not considered in the time-course experiments (Fig. 9B).

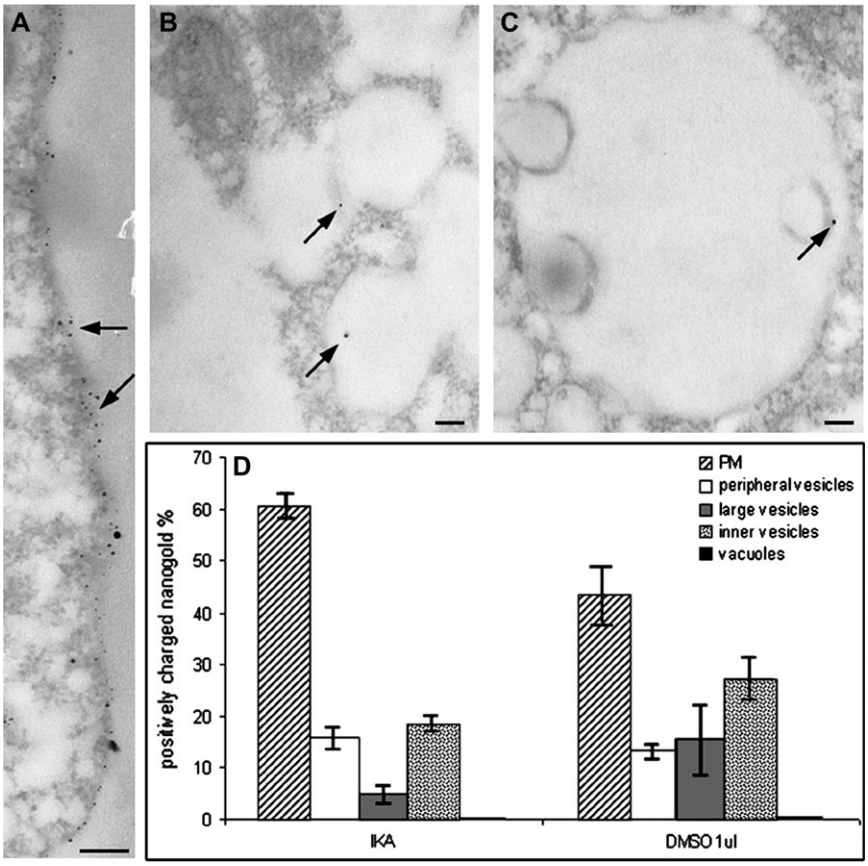

Fig. 8. Compartments labelled by positively charged nanogold and quantitation of the labelled profile during the Ikarugamycin experiment: protoplasts were incubated with IKA to inhibit clathrin-dependent endocytosis. (A) Nanogold accumulated on the plasma membrane and in some areas gold labelling formed clusters immediately below the plasma membrane (see arrows). (B, C) Some nanogold particles were observed in interconnected vesicle compartments (B, see arrow) and MVBs (C, see arrow). (D) Quantitation of particle distribution confirmed TEM observations. Since IKA was suspended in DMSO, the effects of IKA on nanogold internalization were compared with DMSO. IKA inhibited probe internalization and many particles were still found in inner vesicles after IKA treatment, suggesting that most of the traffic involving small inner vesicles was due to clathrin-independent processes bypassing tubular/round vesicles. Standard error (SE) is shown for quantitation data. Bar=100 nm.

To follow the internal sorting of internalized negatively charged nanogold, time-course and pulse experiments were performed (Fig. 9B, C). Quantitative analysis suggested that different endocytotic pathways involved the inner vesicles. During time-course experiments (Fig. 9B), a decrease in negatively nanogold in peripheral vesicles between 5 min and 45 min (P <0.05) was observed while the decrease on the PM and the increase in large and small inner vesicles was not significant, suggesting that the distribution of negatively charged nanogold, reaches an equilibrium after a few minutes of incubation. However, the amount of negatively charged nanogold was significantly lower in peripheral vesicles and significantly higher in inner vesicles (P <0.01) with respect to positively charged nanogold (compare Figs 3B and 9B), suggesting a different involvement of these compartments in the internalization process of the two probes. Moreover, as observed in IKA experiments, again particles were mostly observed on MVBs (Fig. 10A) and interconnected vesicles. Only occasionally was the probe present in round/tubular compartments (Fig. 10B) and ER or Golgi bodies (Fig. 10C). In fact, during time-course, the number of particles in Golgi bodies and ER and the percentage of labelled Golgi bodies remains constant (Fig. 9D, E). However, in ER and Golgi bodies the amount of probe was lower with respect to positively charged nanogold (compare Figs 3C and 9D; Fig. 9E).

The involvement of internal trafficking in negatively charged nanogold internalization and a slowdown or lack of recycling was confirmed by pulse experiments (Fig. 9C). In fact, the number of particles on the PM dropped sharply after 15 min and 45 min (P <0.01), suggesting that negatively charged nanogold was internalized and did not return to the cell periphery. The increase in particles in vacuoles and large vesicles, represented mostly by later compartments (Fig. 10A, B), 15 min after probe removal are not significant. After 45 min, the probe was recycled from the vacuole but did not re-enter the secretory pathways, since it was found in inner vesicles (Fig. 9C). The amount of particles in Golgi bodies and ER and the

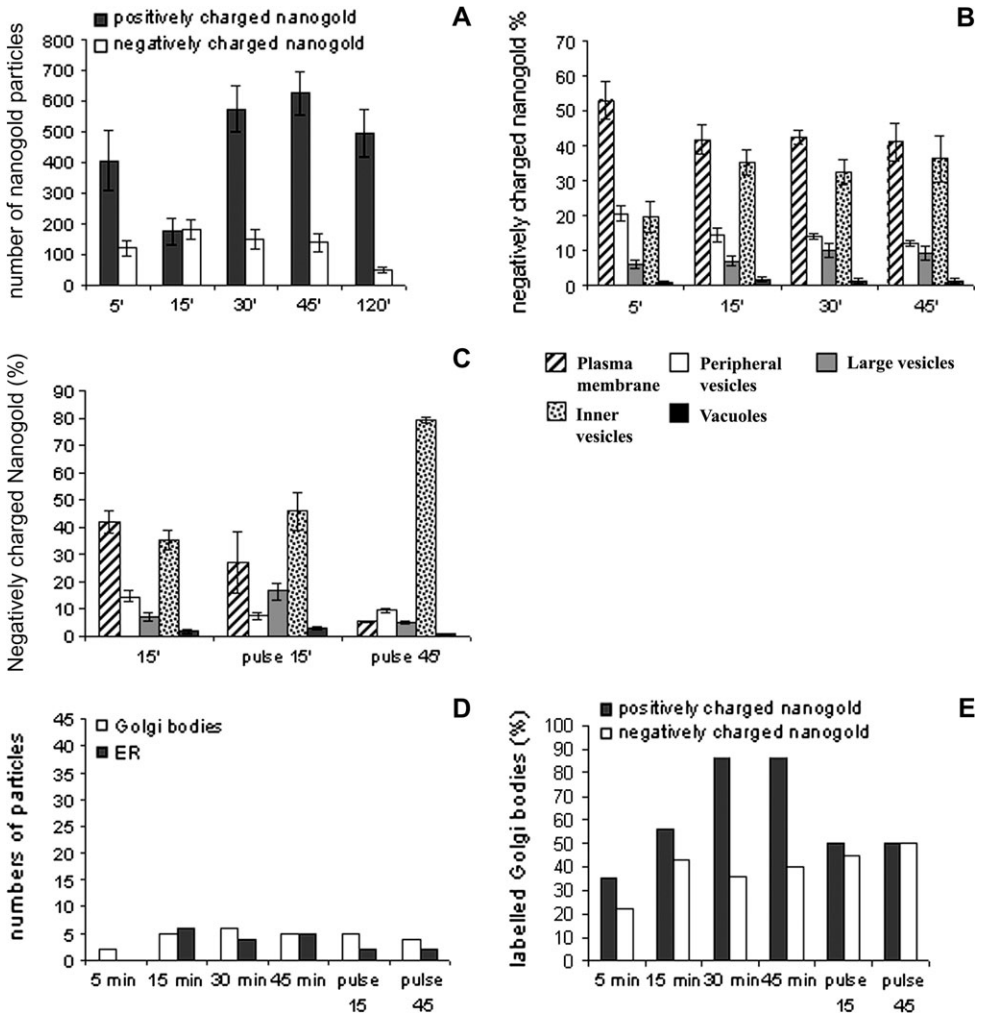

Fig. 9. Quantitation of negatively charged nanogold internalization. (A) Variation in the total amount of particles counted in each sample during the time-course. (B) Distribution of probe in different compartments during the time-course. (C) Distribution of the probe in different compartments and during pulse chase. Quantitation of negatively charged nanogold was performed as for positively charged nanogold. A lesser amount of negatively charged nanogold was found in the cells compared with positively charged nanogold (A); after the uptake, the negatively charged nanogold was mostly delivered to inner vesicles (B, C) and to the degradation pathway, while the recycling to PM is slower or does not occur. (D, E) In ER and Golgi bodies the amount of probe and the percentage of labelled Golgi bodies were lower with respect to positively charged nanogold. The amount of particles in Golgi bodies and ER and the percentage of labelled Golgi bodies remained constant during pulse. Standard error (SE) is shown for each experiments.

percentage of labelled Golgi bodies remain constant during pulse (Fig. 9D, E).

Discussion

In this study, positively charged nanogold was used as a non-specific marker to study the endocytic process. This probe allowed the detailed ultrastructural description of organelles involved in endocytosis. Different compartments similar to those observed in animals, such as putative early endosomes and MVBs, were progressively labelled by the probe during the time-course, suggesting the involvement of these organelles in internalization pathways. However, quantitative analyses showed that putative early endosomes could be a sorting station for degradation or recycling of internalized material. Furthermore, a compartment formed by a network of vesicles was identified as a late endosome by the *Arabidopsis* anti-syntaxin family Syp-21 antibody. Pulse experiments and BFA showed that recycling of the PM is a prominent pathway in the endocytic process with respect to degradation. Energy- and temperature-dependent experiments also showed high recycling activity and suggested the presence of different internalization pathways in protoplasts. This hypothesis was confirmed by experiments with negatively charged nanogold and IKA, a clathrin-dependent endocytosis inhibitor, that did not stop the probe uptake and demonstrated different involvement of organelles.

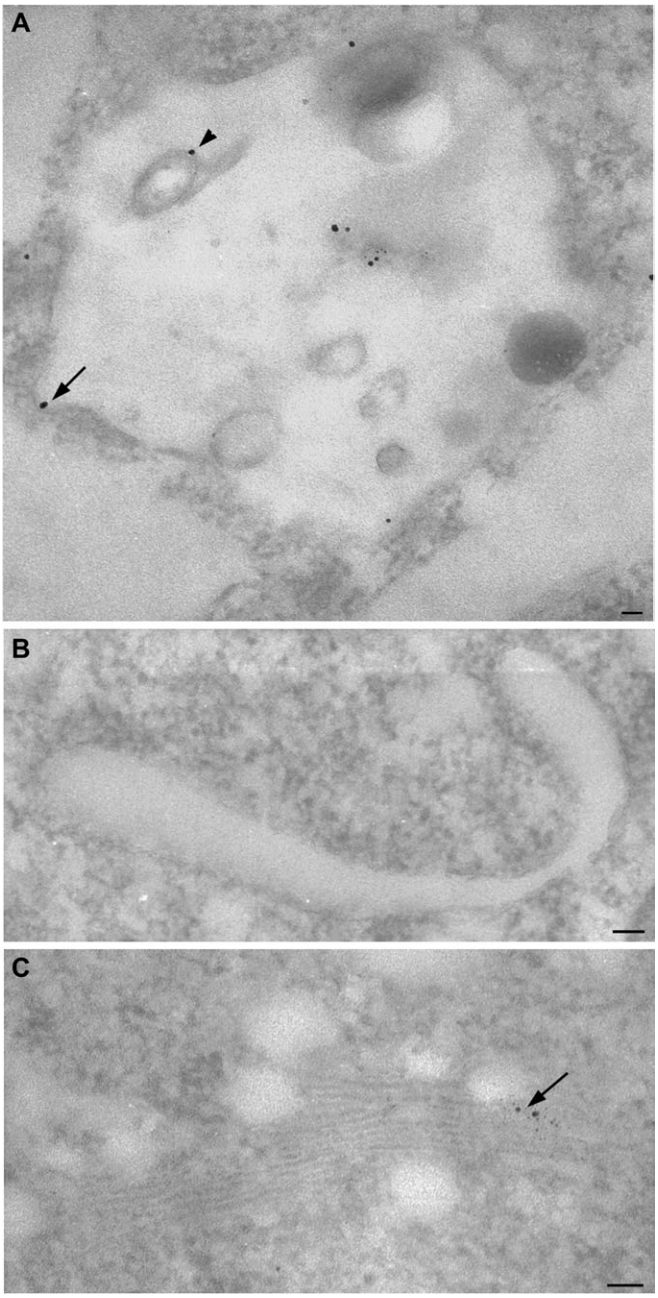

Fig. 10. Compartments labelled by negatively charged nanogold during time-course experiments. In MVBs, the probe labelled delimiting (A, see arrow) and internal membranes (A, see arrowheads). Large tubular vesicles did not show particles (B). Negatively charged nanogold was also observed in Golgi bodies(C, see arrows). Bar=50 nm.

Positively charged nanogold is delivered to degradative and recycling pathways

Incubation of tobacco protoplasts with nanogold for different times enabled us to define the internalization pathways. Different organelles seemed to be involved in the endocytic process. While some were similar to those already described in plants and animals, others had new morphological characteristics. As observed for FM-dyes, staining of the PM with nanogold is immediate (Fig. 1A). After 5 min nanogold was internalized and found within cortical vesicles. During the time-course experiment, the total amount of nanogold in the protoplast increased between 15 min and 30 min after which it was almost constant (Fig. 3A). During the following 45 min and 120 min periods, internalization from the medium and recycling from inner compartments contributed to the presence of particles on the cell surface. After 30–45 min, gold binding sites on the PM were presumably saturated so that the amount of particles in the protoplasts was constant. In time-course experiments, two large morphologically distinct compartments were involved after nanogold internalization. After only 5 min and 15 min the probe became localized in isolated large vesicles (Fig. 1B, C), often showing a tubular structures (Fig. 1E). Later, the amount of particles increased in these membraneous organelles (Fig. 3B) suggesting that they could be a first site involved in internalization after uptake from the PM. Some of these tubular structures were connected to roundish cisternae (Fig. 1F) and resembled the early endosomes described in animal cells. The latter have cisternal regions from which tubules and vesicles seem to emanate (Gruenberg and Stenmark, 2004). Thus, tubular vesicles could be a part of the first compartment involved in internalization, or alternatively, some tubular structures could be similar to recycling endosomes described in animal cells, where the return of internalized material to the PM involves distinct recycling organelles of tubular shape (Sheff *et al*., 1999).

In different plant species, the TGN was recently identified by SCAMP1 and V-ATPase as the first compartment involved in endocytosis (Dettmer *et al*., 2006; Lam *et al*., 2007), so that sorting of internalized PM segments and exocytosis of newly synthesized materials could be done by the same organelle (Dettmer *et al*., 2006). Moreover, other authors have speculated that TGN/early endosomes lack the degradation or recycling sorting function which is associated with another endocytotic organelle (the recycling/sorting endosome) produced by TGN (Geldner and Jurgens, 2006). The tubular-roundish structures of early compartments in tobacco protoplasts are reminiscent of these hypothetical TGN-derived compartments (recycling/sorting endosomes) as suggested by Geldner and Jurgens (2006), rather than of TGN/early endosomes. In fact, like mammalian early endosomes (Gruenberg and Stenmark, 2004), the tubular-round structures of tobacco protoplasts showed a cisternal portion with internal membranes morphologically similar to MVBs (Fig. 1F), suggesting that this organelle may play a role in sorting/recycling to the PM or to degradative pathways. In animal cells, early endosomes develop membrane domains with distinct protein–lipid composition that participate in conveying internalized molecules to their destinations. This amounts to endosome

recycling (Sheff *et al*., 1999) and delivery to MVBs (Gruenberg and Stenmark, 2004). Recycling and degradation pathways are therefore topologically and functionally separate in early endosomes: recycling molecules are observed in the tubular part of this organelle that give rise to tubular recycling endosomes while cisternae may mature into MVBs involved in the degradation pathway. The tubular vesicles and MVBs shown in Figs 1 and 2 could also be derived from maturation of different regions of plant putative recycling/sorting endosomes. In plants, as in animals (Maxfield and McGraw, 2004; Murphy *et al*., 2005), the early compartments are thought to mature into late endosomes, so carrier vesicles could not transport materials between these two permanent compartments. In *Arabidopsis*, different SNARE and Rab GTPases seem to differentiate two populations of endosomes functionally and the partial overlapping of these proteins suggests that early endosomes mature into different late compartments (Ueda *et al*., 2004). In plants, MVBs are believed to contribute to the formation of prevacuolar compartments (PVC; Tse *et al*., 2004) with similar morphology to the late endosomes of animal cells. Late endosomes of mammalian cells are highly pleiomorphic with cisternal, tubular, and multivesicular regions (Gruenberg and Stenmark, 2004).

In tobacco protoplasts, the compartment formed by interconnected vesicles shown in Fig. 2 could be a structure morphologically similar to late endosomes, albeit internal vesicular structures similar to those of MVBs in animals were not observed in this organelle. Furthermore, this compartment was labelled after 30 min of incubation but not after 15 min and gold particles appeared to detach from the membrane (Fig. 2D) probably due to increased acidity in the lumen. This compartment was never connected with the central vacuole in all sections observed, suggesting that it could be a new organelle involved later in the internalization process. It therefore seems that, in tobacco protoplasts, degradative pathways involve both MVBs and interconnected vesicle compartments. Identification of labelled compartments was particularly difficult, since specific markers for endosomes like plant anti-RabGTPase and SNARE specific antibodies are not yet available for plants. Rab-GTPases (Ara7, Ara6, and Rha1) were recently identified in *Arabidopsis* protoplasts and shown to be localized on endosomes (Ueda *et al*., 2001, 2004; Kotzer *et al*., 2004). However, some discrepancies in the localization of these proteins in early and late compartments of the endocytic pathway remain, preventing their use for endosome identification (Ueda *et al*., 2001; Geldner and Jurgens, 2006; Tse *et al*., 2006). *Arabidopsis* syntaxinPEP12p and pea vacuolar sorting receptor BP-80 were used as markers for putative PVCs (daSilva Conceição *et al*., 1997; Li *et al*., 2002). Syp21, that plays a role in lytic vacuolar transport (Foresti *et al*., 2006) involving late post-Golgi compartments (Sanderfoot *et al*., 1998; Foresti *et al*., 2006), was considered. In *Arabidopsis*, it is associated with late reticulo-tubular organelles (PVC; Sanderfoot *et al*., 1998) but was not detected on PM, Golgi, ER, or tonoplast (daSilva Conceição *et al*., 1997). In tobacco protoplasts (Fig. 5), Syp21 antibodies labelled MVBs and interconnected vesicles, also identifying the latter compartment as a late endosome. In fact, tonoplast was never labelled by this antibody, confirming that interconnected vesicles were distinct from the vacuole.

Although quantitative analysis (Fig. 3B) showed that after 30 min, most of the nanogold inside the cell was observed in large vesicles, which included both vesicular/tubular structures and interconnected vesicles, it was also noticed that the vesicular/tubular structures contained most of the probe (compare Figs 1E and 2D). This observation further supports the hypothesis that, though involved later, the vesicular network does not represent the compartment for final accumulation of probe. Nanogold presumably was delivered later into vacuoles. With positively charged nanogold, vacuoles were stained less (Fig. 3B) than with FM-dyes (Bolte *et al*., 2004) probably due to the different properties of the probes. In fact, FM-dyes bind uniformly to the PM, showing all internalization pathways, but positively charged nanogold shows the endocytosis of PM domains binding positively charged particles. The endocytic pathways revealed by charged nanogold suggested that these PM regions are destined mostly to be recycled back to the cell surface rather than to be degraded in the central vacuole. Depending on the differentiation pathways, plant cells may form several kinds of vacuole that differ in size, shape, and function (Jiang and Rogers, 1998; Marty, 1999). The central vacuole is considered to be analogous to lysosomes of animal cells and thus to be involved in degradation pathways (Bolte *et al*., 2004). In animals, late endosomes discharge their contents into lysosomes by direct fusion, thus excluding vesicle traffic (Luzio *et al*., 2000; Katzmann *et al*., 2002). In tobacco protoplasts, as well as in tobacco BY-2 cells (Yamada *et al*., 2005), endosomes appeared to fuse with vacuoles (Fig. 2A, B) in the final step of degradation.

Labelled small vesicles increased during time-course experiments (Fig. 3B): peripheral and small cortical vesicles observed early during nanogold incubation could be involved in traffic from the PM to early compartments or already in recycling. Small inner vesicles, widespread in the cytoplasm, could mediate traffic between endosomes and PM or to and from Golgi and ER; the latter were labelled after 30 min of incubation with nanogold (Figs 1, 3, 6). These organelles are known to be involved in recycling and degradative pathways (Surpin and Raikhel, 2004). The plant Golgi apparatus is regarded as a sorting station: materials from endosomes could be delivered, by the TGN or ER to different types of vacuoles or back to the PM (Jurgens, 2004).

When nanogold was removed after 15 min of incubation in pulse experiments, internalized particles were visible in all the above organelles (data not shown), whereas quantitative analyses (Fig. 6A) suggested that particles are first distributed from the cortical regions into all internal cell compartments. Then a remarkable return to the plasmalemma occurs, probably involving exocytosis (Battey *et al*., 1999) and recycling. Protoplasts are presumably synthesizing new cell walls involving Golgi-derived secretory vesicles, thus contributing to a return of particles to the cell surface. This aspect was confirmed by using Calcofluor that showed an increase in staining of protoplasts with respect to T_0 (data not shown) so suggesting that cell wall synthesis has already started after 30 min. In addition, the poor labelling observed in vacuoles in pulse chase experiments (Fig. 6A) confirmed that recycling could be a prominent pathway, redirecting nanogold to the cell surface, as observed in animals (Goda and Pfeffer, 1988) and supporting the observations of time-course experiments. The low labelling of Golgi and ER with respect to time-course experiments, suggested that recycling pathways probably occur by a fast way that does not involve exocytosis. A direct return of the probe to PM from early compartments, also supports the hypothesis that tubular-round structures could represent the hypothetical TGN-derived compartments in tobacco protoplasts (recycling/sorting endosomes; Geldner and Jurgens, 2006). Pulse chase experiments also suggested that the central vacuole participates in the degradation pathway, as observed in other plant systems (Jiang and Rogers, 1998; Bolte *et al*., 2004). 15 min and 45 min after pulse (of recovery from the pulse), the amount of the probe in the central vacuoles did not change significantly, suggesting the re-entry of probe from the tonoplast in vesicle trafficking. The central vacuole thus appears to be a dynamic organelle in which vesicle traffic to and from other membraneous compartments occurs as observed in other plant cells (Echeverria, 2000) and in animals (Thilo *et al*., 1995). The dynamism of the tonoplast and the firm binding of the probe to negatively charged targets on this membrane, could explain the low level of labelling in the central vacuoles observed in time-course and other experiments.

Inhibition of exocytosis decreased the PM internalization

In plant cells, BFA has been shown to block the secretion of cell wall polysaccharides and proteins (Schindler *et al*., 1994; Kunze *et al*., 1995; Ritzenthaler *et al*., 2002) affecting internal membrane organization: it creates a hybrid compartment, formed by Golgi cisternae merged with ER with the characteristics of both (Emans *et al*., 2002; Nebenfuhr *et al*., 2002; Ritzenthaler *et al*., 2002) and a BFA-compartment arising from TGN and membranes of endocytic-recycling origin (Nebenfuhr *et al*., 2002; Ritzenthaler *et al*., 2002). In addition, in plant cells, different concentrations of BFA can induce the formation of endosome aggregates without involving other compartments (Geldner *et al*., 2003; Tse *et al*., 2006). This different sensitivity could be due to the specific presence of ARF GEF proteins differentially affected by BFA. Moreover, the relationships between exocytosis and endocytosis vary in different cell types (Satiat-Jeunemaitre *et al*., 1996; Baluška *et al*., 2002; Tse *et al*., 2006). Differences in BFA response depend on the physiological state of the secretory and endocytotic systems (Nebenfuhr *et al*., 2002).

Quantitative analysis showed that, in BFA-treated tobacco protoplasts incubated with positively charged nanogold, concentrations of 5 μM affected the early phases of the internalization process (Fig. 6C). In fact, unlike FM4-64 (Emans *et al*., 2002; Bolte *et al*., 2004), BFA significantly inhibited probe uptake and transport to early inner compartments, also contrasting the opposite effect of DMSO. An aspect to be considered regarding discrepancies in FM4-64 uptake in the presence of BFA is that positively charged nanogold only shows some endocytic events in cells. In addition, FM4-64 is inserted in the outer membrane leaflet whereas our probe only binds molecules on the membrane surface, so they probably have different effects on membrane dynamics.

In tobacco protoplasts, the early events of endocytosis of positively charged nanogold, particularly the entry of probe and the traffic between the peripheral region and the inner cell compartments, were related to perturbations of the exocytic pathway. BFA data confirmed internalization of the PM in order to maintain the cell membrane economy, as suggested by the time-course experiments which showed a predominant recycling pathway. Inhibition of exocytosis, therefore, does not require that cells recycle excess secreted PM.

Azide treatment and low temperature affect endocytosis

Sodium azide treatment showed that sodium azide affected inner vesicle traffic. However, otherwise in experiments using nanogold in yeast (Prescianotto-Baschong and Riezman, 1998), energy and temperature controls never produced an overall inhibition of the internalization process: in tobacco protoplasts some labelling was still observed in all the compartments described. This is probably due to glycolysis that occurred because of the presence of sucrose in the medium. With low sodium azide concentrations, the particles accumulated in small vesicles and probe uptake was not inhibited (Fig. 7A). Accumulation of probe in small inner vesicles also affected both recycling pathways, explaining the minor amount of nanogold on peripheral vesicles, and exocytosis as suggested by the low level of labelling in

Golgi and ER (Fig. 7E, F). The slight decrease in nanogold in large vesicles suggested that internalization and sorting in early organelles was not affected, while later, inhibition of trafficking prevented probe from accumulating in late compartments. Particles were thus internalized in peripheral vesicles, transported to early round-tubular vesicles and then sorted to small inner vesicles in which they accumulated because of inhibition of trafficking. High concentrations of sodium azide have a different effect from low concentrations (Fig. 7B), as observed in pollen tubes where internalization of FM-dyes was inhibited in a concentration-dependent manner (Parton *et al*., 2001): at low concentration, cytoplasmic streaming was not arrested, allowing uptake of probe, albeit at a reduced rate, while higher concentration (1 mM sodium azide) inhibited the internalization process. At 1 mM sodium azide, tobacco protoplasts died. The highest concentration of sodium azide which maintained cell viability (500 μM) affected the entrance of nanogold into the cells, as suggested by the significant decrease of the probe in large vesicles. No significant variation of labelling in small inner vesicles suggested the contribution of different internalization pathways not involving large early compartments but rather, small vesicles and central vacuoles. At low and high sodium azide concentrations, no significant variation of labelling on the tonoplast could suggest that a path to the central vacuole was less affected by sodium azide than was recycling. Similarly, in animal cells, recycling endosomes rarely contain fluid phase markers of endocytosis and some clathrin-independent processes do not involve early endosomes but other compartments, such as caveosomes (Nichols and Lippincot-Schwartz, 2001). The analysis of the results of the sodium azide experiments revealed the energy requirements of endocytosis. It is interesting to observe that sodium azide showed a direct pathway between PM and vacuoles. Inhibition of internalization with higher sodium azide concentrations should also affect the amount of nanogold in peripheral vesicles due to the inhibition of recycling, but a significant variation in the number of particles in this compartment was not observed with respect to the control (Fig. 7B).

In the same way, low temperature mainly affected the uptake of probe and its transfer to early compartments, as suggested by a significant increase of particles in the peripheral vesicles and a decrease in large vesicles, but did not inhibit the process as a whole. Nanogold was internalized and distributed to all compartments at a reduced rate, suggesting that low temperature slows the endocytic process but does not stop it (Fig. 7C). As observed for the sodium azide experiments, whereas the presence of the probe in the inner vesicles was not significantly changed, the pathway leading to the large vesicles seemed to be affected, so suggesting the presence of several internalization pathways involving different endocytic organelles. Thus, since it has been observed that clathrin-dependent endocytosis is sensitive to low temperature (Wileman *et al*., 1985; Baluška *et al*., 2002), the differences in nanogold distribution observed in these experiments could be due to the presence of several endocytic processes influenced differently by low temperature.

During cold experiments (Fig. 7D), it was observed that endocytotic processes were rapidly recovered as suggested by the presence of an irrelevant variation with respect to the control (45 min; Fig: 7D).

Ikarugamycin and negatively charged nanogold internalization revealed different endocytic pathways

In plants, clathrin-dependent endocytosis has been considered to be the predominant pathway for the internalization of most PM proteins (Dhonukshe *et al*., 2007), however, clathrin-independent endocytosis was also observed (Holstein, 2002; Son *et al*., 2003; Baluška *et al*., 2004; Borner *et al*., 2005; Martin *et al*., 2005). Ikarugamycin (IKA) is an antibiotic that inhibits uptake of PM via clathrin-dependent endocytosis in animal cells (Hasumi *et al*., 1992; Luo *et al*., 2001) while not affecting surface binding of ligands and internal trafficking. The mechanisms by which IKA inhibits probe uptake seems related to the formation of clathrin-coated vesicles. In fact, after IKA incubation, patches of clathrin heavy chain were observed on the plasma membrane of tobacco pollen tubes (Moscatelli *et al*., 2007).

In tobacco protoplasts IKA inhibited probe internalization as suggested by the accumulation of particles on the cell surface (Fig. 8). It is possible that the quantitative analyses in peripheral vesicles and on the PM were affected by the difficulty of counting nanogold particles in areas of probe accumulation: the number of gold particles in peripheral vesicles could be overestimated with respect to those on the PM. The high level of labelling on the PM (Fig. 8A, D) cannot be due to recycling processes which are limited by the small number of particles in early sorting compartments. The inhibition of probe uptake was confirmed by the low level of particles in large vesicles (Fig. 8D), due particularly to the rare presence of nanogold in round/tubular structures, confirming that clathrin-dependent endocytosis involves this early compartment as a sorting station after internalization. A limited decrease in nanogold particles in inner vesicles with respect to the control could be due to a lack of recycling. On the other hand, the fact that many particles were still found in inner vesicles after IKA treatment suggests that most of the traffic involving small inner vesicles was due to clathrin-independent processes bypassing tubular/round vesicles. Trafficking during clathrin-dependent endocytosis, therefore, only seems to involve inner vesicles marginally, as suggested by the energy and low-temperature experiments. The path from

early to late compartments during the clathrin-dependent process may not involve small vesicles but may occur by maturation of organelles as already suggested (Ueda *et al*., 2004; Yamada *et al*., 2005). The variation of labelling on the tonoplast was not significant (Fig. 8D) suggesting that clathrin-dependent endocytosis did not contribute to a large extent to the degradation pathway. This is also confirmed by the labelling of late compartments by negatively charged nanogold rather than early sorting organelles that are principally involved in recycling the probe to the PM.

The presence of several endocytotic pathways is also suggested by the internalization of negatively charged nanogold. There was less binding of negatively charged nanogold to the PM than positively charged nanogold (Fig. 9); after uptake, negatively charged nanogold was mostly delivered to inner vesicles (Fig. 9), whereas few particles were found in round/tubular compartments. Among large vesicles, most of the probe labelled compartments involved in the degradation pathway such as MVBs and interconnected vesicles (Fig. 10). Interestingly, during time-course experiments, the amount of positively and negatively charged nanogold in large vesicles was not significantly different. Nevertheless, different kinds of large vesicles are involved in the two endocytic pathways. Whereas the positively charged nanogold was observed in round/tubular vesicles, the negatively charged nanogold was, instead, seen inside late compartments. These data, therefore, suggest that negatively charged nanogold is preferentially delivered to the degradation pathway and that recycling to PM is slower or does not occur.

Quantitative analysis of the internalization pathway shown by negatively charged nanogold closely resembled that of positively charged nanogold in the presence of IKA: both showed reduced recycling and an increase in probe in degradative compartments, suggesting that clathrin-independent endocytosis preferentially involves degradation. In animal cells, clathrin-independent endocytosis has been involved in the internalization of pathogens for degradation or to be delivered to the ER or Golgi apparatus (Pelkmans and Helenius, 2003). Moreover, segments of PM binding negatively particles could be involved in internal trafficking through cell organelles such as Golgi bodies and ER that were labelled by the probe. Although it was suggested that the fluid phase endocitic pathways does not induce probe accumulation in the vacuole (Baluška *et al*., 2004), we could not discriminate if the clathrin-independent pathways revealed by our experiments followed fluid-phase endocytic mechanisms.

Acknowledgements

We thank CIMA (Centro Interdipartimentale di Microscopia Avanzata) for technical assistance with TEM and Mr Roberto Cavatorta for photographic support. We thank N Raikhel for providing the SYP21 polyclonal antibody. This work was supported by the FIRST project 2006, financed by the University of Milan.

References

Ang AL, Taguchi T, Francis S, Fölsch H, Murrells LJ, Pypaert M, Warren G, Mellman I. 2004. Recycling endosomes can serve as intermediates during transport from the Golgi to the plasma membrane of MDCK cells. *Journal of Cell Biology* **167,** 531–543.

Baba T, Rauch C, Xue M, Terada N, Fujii Y, Ueda H, Takayama I, Ohno S, Farge E, Sato SB. 2001. Clathrin-dependent and clathrin-independent endocytosis are differentially sensitive to insertion of poly(ethylene glycol)-derivatized cholesterol in the plasma membrane. *Traffic* **2,** 501–512.

Baluška F, Hlavacka A, Samaj J, Palme K, Robinson DG, Matoh T, McCurdy D, Menzel D, Volkmann D. 2002. F-actin-dependent endocytosis of cell wall pectins in meristematic root cells. Insights from Brefeldin A-induced compartments. *Plant Physiology* **130,** 422–431.

Baluška F, Samaj J, Hlavacka A, Kendrik-Jones J, Volkmann D. 2004. Actin-dependent fluid phase endocytosis in inner cortex cells of maize root apices. *Journal of Experimental Botany* **55,** 463–473.

Battey NH, James NC, Greenland AJ, Brownlee C. 1999. Exocytosis and endocytosis. *The Plant Cell* **11,** 643–659.

Bolte S, Talbot C, Boutte Y, Catrice O, Read ND, Satiat-Jeunemaitre B. 2004. FM-dyes as experimental probes for dissecting vesicle trafficking in living plant cells. *Journal of Microscopy* **214,** 159–173.

Borner GH, Sherrier DJ, Weimar T, Michaelson LV, Hawkins ND, Macaskill A, Napier JA, Beale MH, Lilley KS, Dupree P. 2005. Analysis of detergent-resistant membranes in *Arabidopsis*. Evidence for plasma membrane lipid rafts. *Plant Physiology* **137,** 104–116.

daSilva Conceição A, Marty-Mazars D, Bassham DC, Sanderfoot AA, Marty F, Raikhel NV. 1997. The syntaxin homolog AtPEP12p resides on a late post-Golgi compartment in plants. *The Plant Cell* **9,** 571–582.

Dettmer J, Hong-Hermesdorf A, Stierhof YD, Schumacher K. 2006. Vacuolar H^+-ATPase activity is required for endocytic and secretory trafficking in *Arabidopsis*. *The Plant Cell* **18,** 715–730.

Dhonukshe P, Aniento F, Hwang I, Robinson DG, Mravec J, Stierhof YD, Friml J. 2007. Clathrin-mediated constitutive endocytosis of PIN auxin efflux carriers in *Arabidopsis*. *Current Biology* **17,** 520–527.

Echeverrìa E. 2000. Vesicle-mediated solute transport between the vacuole and the plasma membrane. *Plant Physiology* **123,** 1217–1226.

Emans N, Zimmermann S, Fischer R. 2002. Uptake of a fluorescent marker in plant cells is sensitive to Brefeldin A Wortmannin. *The Plant Cell* **14,** 71–86.

Foresti O, daSilva LLP, Denecke J. 2006. Overexpression of the *Arabidopsis* syntaxin PEP12/SYP21 inhibit transport from the prevacuolar compartment to the lytic vacuole *in vivo*. *The Plant Cell* **18,** 2275–2293.

Fowke LC, Tanchak MA, Galway ME. 1991. Ultrastructural cytology of the endocytic pathways in plants. In: Hawes CR, Coleman JOD, Evans DE, eds. *Endocytosis, exocytosis and vesicle traffic in plants*. Cambridge: UK Cambridge University Press, 15–40.

Geldner N, Anders N, Wolters H, Keicher J, Kornberger W, Muller P, Delbarre A, Ueda T, Nakano A, Jurgens G. 2003. The Arabidopsis GNOM ARF-GEF mediates endosomal

recycling, auxin transport and auxin-dependent plant growth. *Cell* **112,** 219–230.

Geldner N, Jurgens G. 2006. Endocytosis in signalling and development. *Current Opinion in Plant Biology* **9,** 589–594.

Goda Y, Pfeffer SR. 1988. Selective recycling of the mannose 6-phosphate/IGF-II receptor to the TGN *in vitro*. *Cell* **55,** 309–320.

Gruenberg J. 2001. The endocytic pathway: a mosaic of domains. *Nature Review* **2,** 721–730.

Gruenberg J, Stenmark H. 2004. The biogenesis of multivesicular endosomes. *Nature Review* **5,** 317–323.

Haas TJ, Sliwinski MK, Martinez DE, Preuss M, Ebine K, Ueda T, Nielsen E, Odorizzi G, Otegui MS. 2007. The Arabidopsis AAA ATPase SKD1 is involved in multivesicular endosome function and interact with its positive regulator LYST-INTERACTING PROTEIN 5. *The Plant Cell* **19,** 1295–1312.

Hao M, Maxfield FR. 2000. Characterization of rapid membrane internalization and recycling. *Journal of Biogical Chemistry* **275,** 15279–15286.

Hasumi K, Shinohara S, Nagamura S. 1992. Endo A. Inhibition of the uptake of oxidized low-density lipoprotein in macrophage J774 by the antibiotic Ikarugamycin. *European Journal of Biochemistry* **205,** 841–846.

Henkel AW, Lubke J, Betz WJ. 1996. FM1-43 dye ultrastructural localization in and release from frog motor nerve terminals. *Proceedings of the National Academy of Sciences, USA* **93,** 1918–1923.

Heslop-Harrison J, Heslop-Harrison Y. 1970. Evaluation of pollen viability by enzymatically induced fluorescence; intracellular hydrolysis of fluorescein diacetate. *Stain Technology* **45,** 115–120.

Holstein SHE. 2002. Clathrin and plant endocytosis. *Traffic* **3,** 614–620.

Jiang L, Rogers JC. 1998. Integral membrane protein sorting to vacuoles in plant cells: evidence for two pathways. *Journal of Cell Biology* **143,** 1183–1199.

Jurgens G. 2004. Membrane trafficking in plants. *Annual Review in Cell Biology* **20,** 481–504.

Katzmann DJ, Odorizzi G, Emr SD. 2002. Receptor down-regulation and multivesicular–body sorting. *Naure Reviews Molecular Cell Biology* **3,** 893–905.

Kim DH, Eu YJ, Yoo CM, Kim YW, Pih KT, Jin JB, Kim SJ, Stenmark H, Hwang I. 2001. Trafficking of phosphatidylinositol 3-phosphate from the *trans*-Golgi network to the lumen of the central vacuole in plant cells. *The Plant Cell* **13,** 287–301.

Kirkham M, Fujiita A, Chadda R, Nixon SJ, Kurzchalia TV, Sharma DK, Pagano RE, Hancock JF, Mayor S, Parton RG. 2005. Ultrastructural identification of uncoated caveolin-independent early endocytic vehicles. *Journal of Cell Biology* **168,** 465–476.

Kotzer A, Brandizzi F, Neumann U, Paris N, Moore I, Hawes C. 2004. AtRabF2b (Ara7) acts on the vacuolar trafficking pathways in tobacco leaf epidermal cells. *Journal of Cell Science* **117,** 6377–6389.

Kunze I, Hillmer S, Kunze G, Muentz K. 1995. Brefeldin A differentially affects protein secretion from suspension-cultured tobacco cells (*Nicotiana tabacum*). *Journal of Plant Physiology* **146,** 71–80.

Laemmli UK. 1970. Cleavage of structural proteins during the assembly of the head of bacteriophage T4. *Nature* **227,** 680–685.

Lam SK, Siu CL, Hillmer S, Jang S, An G, Robinson DG, Jiang L. 2007. Rice SCAMP1 defines clathrin-coated, trans-Golgi-located tubular-vesicular structures as an early endosome in tobacco BY-2 cells. *The Plant Cell* **19,** 296–319.

Li YB, Rogers SW, Tse YC, Lo SW, Sun SS, Jaug GY, Jiang L. 2002. BP-80 and homologs are concentrated on post-Golgi, probable lytic prevacuolar compartments. *Plant Cell Physiology* **43,** 726–742.

Luo T, Fredericksen BL, Hasumi K, Endo A, Garcia JV. 2001. Human immunodefinciency virus type 1 Nef-induced CD4 cell surface down-regulation is inhibited by ikarugamycin. *Journal of Virology* **75,** 2488–2492.

Luzio JP, Rous BA, Bright NA, Pryor PR, Mullock BM, Piper RC. 2000. Lysosome-endosome fusion and lysosome biogenesis. *Journal of Cell Science* **113,** 1515–1524.

Martin SW, Glover BJ, Davies JM. 2005. Lipid microdomains-plant membranes get organized. *Trends in Plant Science* **10,** 263–265.

Marty F. 1999. Plant vacuoles. *The Plant Cell* **11,** 587–599.

Maxfield FR, McGraw TE. 2004. Endocytic recycling. *Naure Reviews Molecular Cell Biology* **5,** 121–132.

Moscatelli A, Ciampolini F, Rodighiero S, Onelli E, Cresti M, Santo N, Idilli A. 2007. Distinct endocytic pathways identified in tobacco pollen tubes using charged nanogold. *Journal of Cell Science* **120,** 3804–3819.

Murphy AS, Bandyopadhyay A, Holstein SE, Peer WA. 2005. Endocytic cycling of PM proteins. *Annual Review of Plant Biology* **56,** 221–251.

Nebenfuhr A, Ritzenthaler C, Robinson DG. 2002. Brefeldin A: deciphering an enigmatic inhibitor of secretion. *Plant Physiology* **130,** 1102–1108.

Nichols BJ, Lippincott-Schwartz J. 2001. Endocytosis without clathrin coats. *Trends in Cell Biology* **11,** 406–412.

Parton MR, Fischer-Parton S, Watahiki MK, Trewavas AJ. 2001. Dynamics of the apical vesicle accumulation and the rate of growth are related in individual pollen tubes. *Journal of Cell Science* **114,** 2685–2695.

Pelkmans L, Helenius A. 2003. Insider information: what viruses tell us about endocytosis. *Current Opinion in Cell Biology* **15,** 414–422.

Pesacreta TC, Lucas WJ. 1985. Presence of a partially-coated reticulum in angiosperms. *Protoplasma* **125,** 173–184.

Prescianotto-Baschong C, Riezman H. 1998. Morphology of the yeast endocytic pathway. *Molecular Biology of the Cell* **9,** 173–189.

Ritzenthaler C, Nebenfuhr A, Movafeghi A, Stussi-Garaud C, Behnia L, Pimpl P, Staehelin LA, Robinson DG. 2002. Reevaluation of the effects of Brefeldin A on plant cells using tobacco bright yellow 2 cells expressing Golgi-targeted green fluorescent protein and COPI antisera. *The Plant Cell* **14,** 237–261.

Samuels AL, Bisalputra T. 1990. Endocytosis in elongating root cells of *Lobelia erinus*. *Journal of Cell Science* **97,** 157–165.

Sanderfoot AA, Ahmed SU, Marty-Mazars D, Rapoport I, Kirkhhausen T, Marty F, Raikhel NV. 1998. A putative vacuolar cargo receptor partially colocalizes with AtPEP12p on a prevacuolar compartment in *Arabidopsis* roots. *Proceedings of the National Academy of Sciences, USA* **95,** 9920–9925.

Satiat-Jeunemaitre B, Cole L, Bourtet T, Howard R, Hawes C. 1996. Brefeldin A effects in plant and fungal cells: something new about vesicle trafficking? *Journal of Microscopy* **181,** 162–177.

Schindler T, Bergfeld R, Hohl M, Schopfer P. 1994. Inhibition of Golgi apparatus function by Brefeldin A in maize coleoptiles and its consequences on auxin-mediated growth, cell wall extensibility and secretion of cell wall protein. *Planta* **192,** 404–413.

Sheff DR, Daro EA, Hull M, Mellman I. 1999. The receptor recycling pathways contains two distinct populations of early endosomes with different sorting function. *Journal of Cell Biology* **1,** 123–139.

Son O, Yang HS, Lee HJ, Lee MY, Shin KH, Jeon SL, Lee MS. 2003. Expression of *srab7* and *SCaM* genes required for endocytosis of *Rhizobium* in root nodules. *Plant Science* **165,** 1239–1244.

Surpin M, Raikhel N. 2004. Traffic jams affect plant development and signal transduction. *Nature Review* **5,** 100–110.

Tanchak MA, Griffing LR, Mersay BG, Fowke LC. 1984. Endocytosis of cationized ferritin by coated vesicles of soybean protoplasts. *Planta* **162,** 481–486.

Tanchak MA, Rennie PJ, Fowke LC. 1988. Ultrastructure of the partially coated reticulum and dictyosomes during endocytosis by soybean protoplasts. *Planta* **175,** 433–441.

Thilo L, Stroud E, Haylett T. 1995. Maturation of early endosomes and vesicular traffic to lysosomes in relation to membrane recycling. *Journal of Cell Science* **108,** 1791–1803.

Towbin H, Staehelin T, Gordon J. 1979. Electrophoretic transfer of proteins from polyacrylamide gels to nitrocellulose sheets. Procedure and some applications. *Proceedings of the National Academy of Sciences, USA* **76,** 4350–4354.

Tse YC, Mo B, Hillmer S, Zhao M, Lo SW, Robinson DG, Jiang L. 2004. Identification of multivesicular bodies as prevacuolar compartments in *Nicotiana tabacum* BY-2 cells. *The Plant Cell* **16,** 672–693.

Tse YC, Lo SW, Hillmer S, Cupree P, Jiang L. 2006. Dynamic response of prevacuolar compartments to Brefeldin A in plant cells. *Plant Physiology* **142,** 1442–1459.

Ueda T, Yamaguchi M, Uchimiya H, Nakano A. 2001. Ara6, a plant unique novel type Rab GTPase, functions in the endocytic pathway in *Arabidopsis thaliana*. *EMBO Journal* **20,** 4730–4741.

Ueda T, Uemura T, Sato MH, Nakano A. 2004. Functional differentiation of endosomes in *Arabidopsis* cells. *The Plant Journal* **40,** 783–789.

Uemura T, Ueda T, Ohniwa RL, Nakano A, Tekeyasu K, Sato MH. 2004. Systematic analysis of SNARE molecules in *Arabidopsis*: dissection of the post-Golgi network in plant cells. *Cell Structure and Function* **29,** 49–65.

Wileman T, Harding C, Stahl P. 1985. Receptor mediated endocytosis. *Biochemical Journal* **262,** 19404–19413.

Yamada K, Fuji K, Shimada T, Nishimura M, Hara-Nishimura I. 2005. Endosomal proteases facilitate the fusion of endosomes with vacuoles at the final step of the endocytotic pathways. *The Plant Journal* **41,** 888–898.